Applied Energy 277 (2020) 115603

Contents lists available at ScienceDirect

Applied Energy

journal homepage: www.elsevier.com/locate/apenergy

On the origin of degradation in fuel cells and its fast identification by applying unconventional online-monitoring tools

Vanja Subotić [a,*], Norbert H. Menzler [b], Vincent Lawlor [c], Qingping Fang [b], Stefan Pofahl [c], Philipp Harter [a], Hartmuth Schroettner [d], Christoph Hochenauer [a]

[a] Institute of Thermal Engineering, Graz University of Technology, Inffeldgasse 25/B, 8010 Graz, Austria
[b] Forschungzentrum Jülich GmbH, Institute of Energy and Climate Research (IEK), 52424 Jülich, Germany
[c] AVL List GmbH, Hans-List-Platz 1, 8020 Graz, Austria
[d] Institute for Electron Microscopy and Nanoanalysis, Graz University of Technology, Steyrergasse 17, 8010 Graz, Austria

ARTICLE INFO

Keywords:
Solid Oxide Fuel Cell (SOFC)
Online monitoring
Degradation
State of the Health (SoH)

ABSTRACT

The key advantage of solid oxide fuel cells (SOFC) – high fuel flexibility – still remains the main challenge disturbing their stability, reliability and durability. Specific operating conditions induce and accelerate various degradation mechanisms and reduce the overall fuel cell lifetime. Identifying and predicting the onset of degradation at the preliminary stage is of crucial importance, in order to provoke appropriate countermeasures and to prolong the service time of the fuel cell technology. This is not possible when using available conventional monitoring tools. When employing appropriate online-monitoring tools the principle of which differs from the most common measurement of a linear stationary system, relevant information about the occurring failure modes can be obtained. An example for it is a total harmonic distortion (THD) tool, which is based on identification of the system non-linearity and its alternation from the stable state. Taking this into account, this study moves from the traditional concepts and we show that: (i) non-conventional methodologies can be used to identify relevant failure modes at their preliminary stage, (ii) it is possible to in-operando differentiate individual degradation mechanisms, and (iii) advanced unconventional online-monitoring tools are time-efficient and required measuring time can be reduced by factor up to 20.

1. Introduction

The development of commercial solid oxide fuel cell (SOFC) systems and their market acceptance require fulfillment of key criteria for long-term stability availability, reliability and durability under "real-world" operating conditions [1]. However, when operating SOFC under operating conditions typical for real application, different failure modes can occur such as electrode degradation based on high fuel and air utilization, carbon deposition [2,3], load cycles, local hot spots caused by high temperature differences, various impurities, or even unpredicted shut-down [4–8]. Moreover, degradation in system components, e.g. reformer and/or effects from the controlling of aging systems, e.g. control lags, overshoots, etc. can also induce system degradation [3,9]. All the mentioned failure modes can accelerate degradation processes and influence the overall operation, which can further result in irreversible damages and strongly reduced remaining useful lifetime [10]. The fundamental understanding of degradation mechanisms and the most important – the possibility for the in-operando identification of degradation at an early stage – are crucial factors to ensure undisturbed operation of SOFCs under a variety of operating conditions and thus to extend the lifetime of this technology [11,12].

Until now, the state-of-the-health (SoH) methods mainly focus on simple methodologies such as polarization curve measurement and electrochemical impedance spectroscopy (EIS) [13,14]. Further possibility is prediction of the cell performance applying simulations based on neural networks [15] or multi-physical models [16,17]. Electrochemical impedance spectroscopy is the method usually applied to analyze processes that occur within electrochemical systems and to deconvolve them [18–20]. Recently, distribution of relaxation times analysis (DRT) is used to split the information obtained from the EIS data according to their time constants [21–23]. When a system operates under safe conditions representing a degradation-free mode, it represents a linear system. Linearity means that a perturbation signal and its response are correlated by linear differential equation [24]. In the case of system linearity, electrochemical impedance spectroscopy represents an appropriate method for analysis of the electrochemical performances of the system under operation. In this case, the amplitude should be as

* Corresponding author.
E-mail address: vanja.subotic@tugraz.at (V. Subotić).

https://doi.org/10.1016/j.apenergy.2020.115603
Received 15 May 2020; Received in revised form 8 July 2020; Accepted 24 July 2020
Available online 5 August 2020

low as possible in order to retain the system linearity. In the opposite to this, high amplitude perturbations result in high signal-to-noise ratio thus increasing the signal quality. For the purpose of linearity assessment, total harmonic distortion (THD) method or non-linear frequency response analysis (NFRA) is used [25]. It shows distortion of the measured impedance spectra by means of higher harmonics (THDA) or higher order frequency response functions generation (NFRA), which are mainly caused due to the high amplitude perturbations. In [26] non-linear frequency response analysis was performed by applying AC-amplitudes in the range of between 12% and 50% of the DC-signal, when investigating membrane flooding and dehydration of polymer electrolyte fuel cells (PEM), as well as CO-poisoning. The analysis of higher order harmonics gave an insight into the processes, which were not observable by using only first order frequency response function. Thus, it is shown that NFRA can be a useful tool to get a better insight into the processes within low temperature fuel cells. Moreover, the same method, when applying it in the range between 2.5 Hz and 15.8 Hz gives information related to the oxygen reduction reaction in the proton exchange membrane fuel cells [27]. Using the same principle on direct methanol fuel cells (DMFC), simulations showed that THD spectra correlate to the methanol concentration in a monotonous manner [28]. In [29] the following frequencies were indicated to correlate to the specific failure modes in PEM cells: 163 Hz to hydrogen starvation achieving approximately 4% of THD, 153 Hz to anode drying conditions with 4% THD, 83 Hz and 12% THD to anode flooding, and 201 Hz and 12% THD to cathode flooding. For high temperature PEMs, the frequencies of 15 Hz and 25 Hz are identified to indicate air starvation, while hydrogen starvation may be associated with the frequency of 15 Hz [30]. Moreover, 6 kW SOFC-stacks were examined on fuel starvation, showing the THD peaks higher than 1% [31]. These peaks are observable while altering operating conditions, until the steady-state for the new conditions is reached. With regards to the studies mentioned, a high current amplitude was superimposed to the system, in order to bring it into the non-linear state and thus to get additional information about the ongoing processes. Nevertheless, in comparison to other studies, which use high amplitudes to provoke the non-linearities in low-temperature fuel cells, this study aims to identify non-linearities that are caused by undesired deviations from the system steady state, while operating the system under stationary conditions and superimposing the amplitude low enough to do not induce a non-linear state.

Scope of this study

A fast determination of degradation in SOFCs at the preliminary stage and identification of different failure modes that simultaneously occur is not available in the literature according to the best of the authors knowledge. In the present work we show how unconventional technique can be applied to monitor and even predict state-of-the-health of the SOFC cells. For that purpose we divided the aims of the study like the following: (i) to evaluate the impact of specific degradation mechanisms that are likely to appear during the real-world system operation, (ii) to accelerate specific degradation mechanisms, and (iii) to apply advanced characterization methods for the effective in-situ identification of intentionally caused degradation. The failure modes to be examined are related to both the fuel and the air electrode. The impact of the induced degradation modes on the electrochemical cell performance and the cell's microstructure is examined in detail. Fuel starvation caused by high fuel utilization (FU) and carbon depositions caused by low S/C-ratio during the steam reforming process were introduced to examine the behavior and the subsequent degradation of the fuel electrode. On the air electrode, air starvation was imposed during the operation at high load to investigate the possible degradation.

For the better insight into different techniques, we compare the non-conventional methodology with the results observed while applying the conventional electrochemical impedance spectroscopy, for which in specific cases a very long measurement duration (higher than 25 min) is required. The advanced approach represented in this study helps to reduce the overall measuring time down to only several minutes, since the non-linear behavior of different failure modes is necessary to be determined only for specific frequencies. Identifying those specific frequencies is a demanding process. However, when the identification procedure is finished for a specific cell type, only the selected specific frequencies are required to be known for the future measurements, thus reducing the wide frequency range and the measuring time. Moreover, this approach enables to obtain more detailed information on specific processes within electrochemical systems by separating them, thus improving the reliability and durability of high temperature fuel cell systems. The SoH method shown gives the relevant information on the system behavior, which represents a step forward needed to create a holistic prognostic and control system. Its application offers a great predictability of various processes and eventual failure modes that may arise.

This study is focused on investigation of large high-temperature solid oxide fuel cells, which significantly increases the complexity of the measurement procedure. This is of crucial importance, since such cells are employed in stacks and real systems, and all the knowledge gained on this stage can further be used for system operation. The SOFCs used are in-house made, thus giving the authors the entire knowledge about the cell microstructure, morphology changes that are expected to be observed under specific operating conditions and in general, the expected cell behavior. The results observed are of great interest to obtain a deeper insight into the processes and degradation of SOFC cells and to predict them in a very short measurement time.

2. Experimental setup and methods

For the purpose of this study, large anode-supported solid oxide fuel cells (ASC) with an active surface of 81 cm^2 manufactured by Forschungzentrum Jülich were employed. Since different degradation mechanisms were examined, a number of cells was used. All the cells were initially tested under reference operating conditions (H_2/N_2 mixture on the fuel electrode and synthetic air on the air electrode) in order to compare their reference performances. The maximum deviation observed was ±3%. Afterwards, the operating conditions were adjusted in order to promote the tailored degradation mechanisms.

Fuel cell fabrication. The anode-supported solid oxide fuel cells were manufactured in the following sequence: the support is tape cast based on a slip composed of the appropriate amounts of raw powder (nickel oxide, Mallinckrodt-Baker, USA and with 8mol% yttria stabilized zirconia (8YSZ), UCM, Germany), solvents, dispersing agents, binders and plasticizers [32,33] with a doctor-blade on a polymeric support tape. After drying and cutting by knife or stamping, the support is pre-sintered at temperatures >1200 °C for 5 h. Afterwards, the anode, composed of NiO and 8YSZ (Tosoh, Japan) is printed via screen printing on the support. The anode is dried and calcined at 1000 °C to ensure a smooth surface for the next coating steps. The 8YSZ electrolyte (Tosoh, Japan) is also screen printed and dried. The three layer system is co-fired at 1400 °C for 5 h to ensure electrolyte gas-tightness. The overall shrinkage is approximately 17% linearly. During the high-temperature sintering the multi-layered structure bends towards the substrate. Thus, to receive flat samples the component is flattened at 1350 °C by applying a load on top of each cell. This flattening step is done directly in one step after the electrolyte densification in a specialized furnace. After cooling down, the samples are cut to the desired size by laser cutting. To mitigate interdiffusion between the electrolyte and the cathode a barrier layer composed of gadolinia-doped ceria (GDC, Treibacher, Austria) is screen printed, dried and sintered at 1300 °C for 3h. This temperature ensures sufficient adherence to the 8YSZ and reasonable densification to avoid interdiffusion with cathodic elements. It is also low enough to hinder complete interdiffusion between the 8YSZ and

the GDC. For more details we refer to [34]. Finally, the cathode is screen printed on the GDC and sintered at 1080 °C for 3h. The cathode material is a mixed ionic-electronic conducting LSCF perovskite ($La_{0.58}Sr_{0.4}Co_{0.2}Fe_{0.8}O_3$- δ) made in house. The active cathode area is $90 \times 90\,mm^2$ on $100 \times 100\,mm^2$ squared cells.

Experimental setup and electrochemical characterization techniques. The ASC-SOFCs, the manufacturing of which is described above, were installed in a ceramic cell housing. The anode side was contacted with nickel mesh, while the cathode side was contacted with platinum mesh. The anode was fed with (i) H_2/N_2 mixture to investigate fuel starvation, and (ii) $CH_4/H_2O/N_2$ mixture to investigate internal steam-reforming and its impact on the anode degradation. The partial pressures of single gas components mentioned above were varied in order to induce the desired failure modes and controlled by means of separate mass flow controllers. The cathode side was supplied with synthetic air, the amount of which was stepwise reduced during the cell loading to obtain more information on air starvation phenomenon and its influence on the cell degradation. The operating temperature was set to 800 °C. During the entire operating time, temperature was measured in a ceramic housing on 14 different points. The analysis of the gas mixture at both the anode inlet and outlet was performed using a gas analyzer. In order to analyze the electrochemical performance of the polarized cells, the DC galvanostatic technique was applied and an AC sinusoidal amplitude (4% of the DC value) was superimposed for the purpose of the electrochemical impedance spectroscopy (EIS). Electrochemical impedance spectroscopy measurements were carried out in a frequency range from 10 kHz to 100 mHz using an impedance analyzer with a 20 V/30 A booster and an option to isolate total harmonic distortion (THD) spectra. THD reflects the non-linear behavior of the system under investigation and in this sense it refers to a ratio between two relevant signal response amplitudes: a sum of all higher harmonic frequencies and the fundamental frequency. In this study operating current was controlled and the voltage was measured. Thus, the THD analysis is related to the voltage response. Because of the defined current range of 30 A for the device used, the operating parameters such as volumetric flow of the fuel used and its composition were chosen and distinctly reduced to bring the maximum cell current down to 30 A at 0.7 V. It is important to mention that all the data presented here are the measured ones, without applying data post-processing.

Microscopic analysis. Small sample areas of approximately $1\,cm^2$ were broken out carefully from the regions of interest of the cell and fixed on a sample holder for the investigations in the electron microscope. The samples are sufficiently conductive. Thus, their surfaces were investigated in a as delivered condition, unchanged, without coating with a metal or carbon film. That would reduce the sensitivity for the carbon detection and also eliminate the low contrast differences in material contrast. All SEM (semi electron microscope) investigations were performed in a ZEISS Ultra 55 Field Emission Scanning Electron Microscope (FESEM) in the high vacuum mode at 10keV excitation energy. Secondary Electron (SE) Images acquired with the SE2 detector (Everhart Thornley Detector — ETD) and SEI Secondary In-lens Detector show topographic contrast. Backscattered Electron (BSE) Images acquired with the HDAsB detector (High Definition Angle Selective Backscatter Electron Detector) show material (z-contrast) and additional orientation contrast (especially in the images of the cross sections/BIB cuts). The Energy Dispersive X-ray (EDXS) spectra were acquired with an EDAX Super Octane Silicon Drift Detection System (Energy Resolution of about 123eV @ Mn Ka) equipped with a silicon-nitride window for best sensitivity in the low energy region (carbon signal). For a better understanding and interpretation of the EDXS spectra, some additional Monte Carlo Simulations using Casino v2.42 at a spot diameter of 2 nm were made. The interaction volume and backscatter coefficient of the backscattered electrons and the depth of X-rays depending on their energy were simulatede. For the simulation of nickel a density of $8{,}9\,g/cm^3$ was used. Due to different referenced literature values for the density of zirconium oxide a mean value of $6\,g/cm^3$ was applied. Due to their low conductivity several samples were investigated in an Environmental Scanning Electron Microscope (FEI Quanta 200 ESEM) in the low vacuum mode at 100 Pa with air as an imaging gas at an acceleration voltage of 20kV. Instead of the high vacuum ETD in the low vacuum the so called Large Field Detector (LFD) was used to acquire a secondary electron image. Backscattered electron images were acquired with the so called Solid State Detector (SSD). The EDXS spectra were acquired with an EDAX Genesis Si–Li-Detector. For the cross sections a small region of interest of the cell is clued on a so called blade for our investigations we used blades made of tungsten with a little overhang. This blade is transferred into the Gatan Ilion Broad Ion Beam Milling system (BIB or Slope Cutter). The overhang of the sample is milled by low energy argon ions, producing an artifact- and damage-free surface for subsequent investigation techniques, where the signal is generated near the surface (Low Energy FESEM, EDXS, EBSD).

3. Results and discussion

With an aim to prove the applicability of the methodology used for identification of various failure modes at their preliminary stage, three different degradation mechanisms were purposefully induced. They are described in detail in the following.

3.1. Fuel starvation

When operating SOFC stacks under real-world conditions, high fuel utilization (FU) is desired in order to maximize the overall efficiency for systems without anode recirculation. Fuel utilization is equal to the reciprocal of fuel stoichiometry as well as to theoretical needed fuel in an ideal case and the provided fuel multiplied by 100. It is a very important parameter for characterization of the stack performance [35]. High fuel utilization can, however, cause fuel starvation and thus accelerate the cell degradation, which is mainly based on undesired reoxidation of the Ni-catalyst and possible mechanical damage of the cell, as a consequence [35].

In order to enable detailed insight into the problematic of high fuel utilization within large SOFCs, FU was varied in the present study between 15% and 92% at the critical operating voltage of 0.7 V for single cells, as can be seen in Fig. 1(b). The fuel utilization is determined by the gas analysis performed at the anode inlet and the anode outlet, thus excluding the possibility of measuring FU as a function of the cell length. Hydrogen was used as a fuel, and its amount in nitrogen was reduced to increase FU at the specific voltage, while the overall volumetric flow on the anode side remained unchanged. For instance, when using fuel mixture of 45% H_2 in N_2, the fuel utilization was approximately 18% at 0.7 V. In this case, the maximum power of approximately $500\,mA/cm^2$ was achieved, which corresponds to approximately $420\,mW/cm^2$, as visible in Fig. 1(a). FU was increased up to 85% by decreasing hydrogen amount down to 10 vol% and thus the power density to $200\,mW/cm^2$; FU further increased to 90% by reducing the hydrogen amount further towards 5 vol% and the maximum achievable power at 0.7 V down to $120\,mW/cm^2$. Regarding this, the overall electrochemical performance of the SOFCs used significantly varied. Fig. 1(c) shows the evolution of the impedance spectra measured under four different current densities, under which the effect of increasing fuel utilization on the cell performance and polarization losses becomes visible when supplying a fuel mixture of H_2/N_2=10/90 to the anode. Under operating conditions at which FU<70%, increasing current density results in decreasing losses, since activations losses get smaller and ohmic losses remain almost unchanged. When significantly increasing the fuel utilization, concentration losses occur, since the fuel transport is not ensured to all the reaction zones. Therefore, the fuel shortage or fuel starvation locally occur. This effect becomes

visible at current densities higher than 250 mA/cm^2 in the specified testing regime, as shown in Figs. 1(c) and 1(d). Impedance spectra and thus the process losses significantly increase especially in the range of middle and high frequencies. The impedance spectra evolution with the increasing current density and thus increasing fuel utilization shows increasing ohmic resistance at high frequencies (from 7.8 mΩ at 250 mA/cm^2 to 8.72 mΩ at 289 mA/cm^2), which can be associated with the changes of the Ni catalyst. Operation under hydrogen depletion conditions for a certain time led to reoxidation of Ni catalyst in the anode as well as to oxidation of the Ni contact mesh, which was verified by microscopic analysis based on SEM- and EDX-analyses, as shown in Fig. 2. NiO is not conductive and not able to act as a catalyst for chemical reactions, in comparison to pure Ni, which thus leads to increase of the ohmic resistance. At this stage, slight Ni reoxidation occurred (see Fig. 2(b)) that can be reversed and does not accelerate the mechanical electrolyte degradation. In the opposite, when operating SOFC under degradation-free conditions, providing sufficient amount of hydrogen, no changes of Ni mesh microstructure are observable. Additional degradation mechanism observed was Ni-agglomeration, as shown in Fig. 2(a). Frequent Ni oxidation and reduction were also observed to occur during the fuel starvation experiments in [10], in which the anode side was composed of Ni/GDC and fuel starvation was induced by interrupting gas supply for 1 or 2 h. In opposite to the present study, in the study mentioned it was stated that redox cycles induced strong cathode degradation that provoked performance deterioration, which can be impacted by the GDC electrolyte. Nevertheless, by employing the anode-supported (ASC) solid oxide fuel cell type specified in our study, intense Ni oxidation could result in irreversible degradation, because of which the identification of the degradation at the early stage is of crucial importance for the specified SOFC type, in order to guarantee the desired state of the health. When employing conventional EIS technique, depending on the data quality and thus the set parameters (e.g. frequency range, number of points per decade, number of measurements per frequency, etc.), one measurement can take even more than 20 or 30 min. For example, when investigating very slow processes, for which the measurements are required to be carried out down to very low frequencies, e.g. 1 mHz. This time period is, however, too long to prevent very fast degradation that takes less than 10 min, when e.g. critical operating conditions, like high FU occur. It is therefore necessary to employ advanced methods that enable very fast degradation identification at its preliminary stage, such as THD methodology illustrated in Fig. 1(d). Results obtained while inducing hydrogen starvation indicated non-linear occurrences mostly in the frequency range <20 Hz, while the total harmonic distortion was observed to be between 3% and 6%.

The results are compared for 4 different operating current densities: 100 mA/cm^2, 200 mA/cm^2, 250 mA/cm^2 and 270 mA/cm^2. During the operation at 100 mA/cm^2, the cell was operated under stationary degradation-free conditions. Under such conditions, water vapor is produced in an electrochemical reaction of hydrogen oxidation along the cell and the reactant–product exchange within the cell takes place in an undisturbed manner. The measured data for this case are indicated by gray line, which shows almost no distortion for the frequencies higher than 0.5 Hz. At frequencies lower than 0.5 Hz slight distortion with a maximum values of 1% is observed. This is because of the cell size, which results in non-uniform temperature and gas (both reactant and hydrogen) distribution along the cell, and the effect of which is visible at lower frequencies [36]. Thus, 1% distortion is to be considered as a threshold value in the low-frequency range. Increasing the operating current density up to 200 mA/cm^2 (illustrated with green line), signal distortions started to occur at the frequencies lower than 2 Hz, achieving the maximum amplitude of 3% at 0.1 Hz. Further increase of the current density increased the signal distortion and extended the frequency range. Operating the cell at 250 mA/cm^2 results in FU=80% and visible fuel starvation. An increasing THD value was observed in the entire frequency range; but especially at frequencies lower than

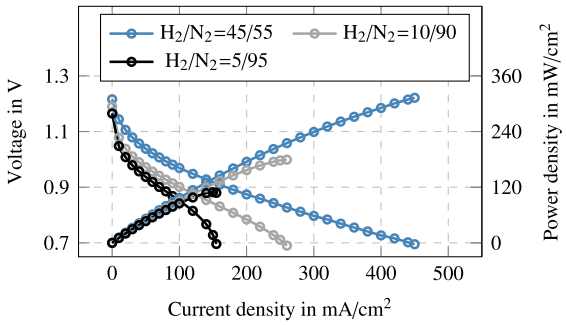

(a) Comparison of polarization curves.

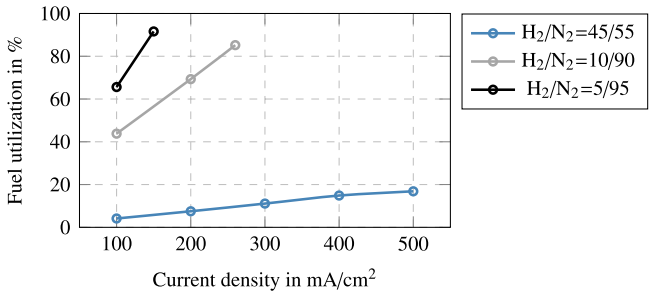

(b) Comparison of fuel utilization values.

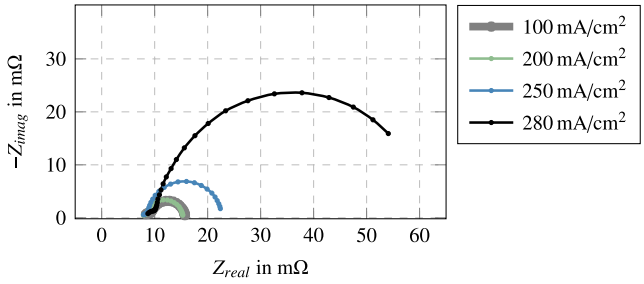

(c) Comparison of EIS spectra measured for H_2/N_2=10/90.

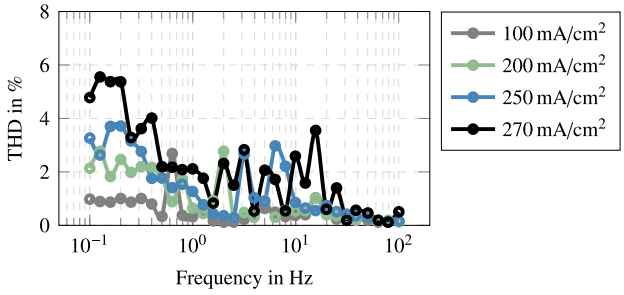

(d) Comparison of THD spectra measured for H_2/N_2=10/90.

Fig. 1. Comparison of cell performance by reducing hydrogen quantity in nitrogen at a constant fuel flow, thus inducing fuel starvation effect at the operating temperature of 800 °C.

5 Hz. The maximum distortion of 4% was observed. This effect was distinctly more pronounced when increasing the FU up to approx. 85% and the current density up to 270 mA/cm^2. Very strong distortion of almost 4% was observed already at 20 Hz, the value of which increased with the decreasing frequency. The changes in the anode morphology observed as oxidized and agglomerated Ni-surface, which occurred as a consequence of fuel starvation, are shown in Fig. 2. In Fig. 2(a) the surfaces marked with a black surface clearly show very large Ni-particles, for which grain boundaries of individual Ni-particles are

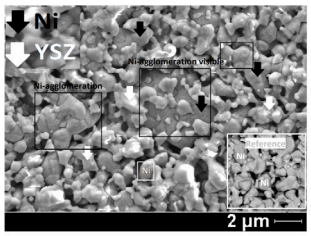

(a) Ni-agglomeration of the anode surface.

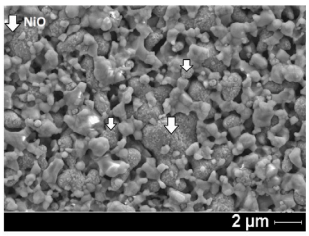

(b) Ni-reoxidation of the anode surface

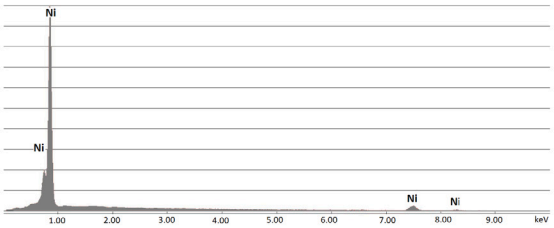

(c) EDX for Ni-surface observed in Fig. 2a.

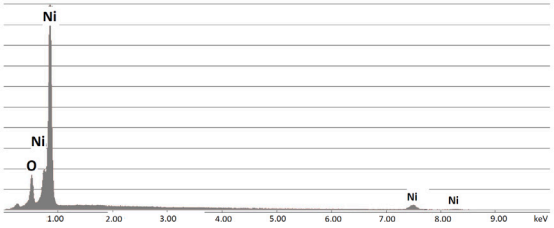

(d) EDX for NiO-surface observed in Fig. 2b.

Fig. 2. SEM and EDX images of the anode surface observed after fuel starvation experiment.

visible. This refers to their agglomeration. The surface within the white square shows the individual Ni-particle, as expected to be before Ni-agglomeration occurs. In addition, a sample of the reference anode is shown in the lower right corner in the same figure.

3.2. Air starvation

A further important parameter that can restrict power generation and accelerate degradation in SOFC systems is insufficient air supply; this occurs in the case when current is drawn from the cell, but the air supply is inhibited. The effects of the insufficient air supply can be determined by non-linear reduction of the cell power, as can be seen in Fig. 3(a). Detailed electrochemical analysis shows arising of the third semi-circle during the impedance spectroscopy measurements when reducing air supply, as represented in Fig. 3(b). The third semi-circle appears only in the case of air starvation, when provoking it on the ASC cells used in this study, thus referring to additional diffusion losses appearing on the cathode side. When intensifying the air starvation by increasing operating current towards critical operating point at which concentration losses significantly increase and cell power reaches a rapid drop towards zero, the ohmic losses increase by almost 50%, as can be seen in Fig. 3(c) for which air supply on the cathode side was set to 0.5 SLPM. Loading the cell at 100 mA/cm^2, the ohmic resistance amounts approximately 5 mΩ, whereby increasing the current density up to 150 mA/cm^2 increases the ohmic losses up to approximately 7.5 mΩ. Under same conditions, the third semi-circle increases abruptly thus implying very high process resistances at low-frequencies, referring simultaneously to slow processes and possible mechanical damage of the cathode. The long-term operation under accelerated degradation conditions, thus considering several hours operation under very low air and thus oxygen quantity at high current density, which consequently decreased the voltage down to zero, caused mechanical degradation of the cathode surface and delamination of the cathode and barrier layer. At the operating current of 150 mA/cm^2, the theoretical air utilization accounts approximately 42%. However, the possibility of the leakage occurrence and undesired air losses must be considered because of the low volume flow, which can be estimated with a maximum of 0.2 SLPM. If the losses account 0.2 SLPM, the air utilization is calculated to be 70%. This can also cause non-uniform air distribution and local starvation effects can occur, which lead to a subsequent cathode degradation. Degradation effects were observed by post-mortem analysis, as can be seen in Figs. 4(a) and 4(b). As already mentioned, the cathode side was contacted with Pt-mesh, which is placed on the upside of the cell and mechanically loaded to improve the overall contact. Because of the specific mesh density, the contacting points were distributed along the cathode. It is likely that on several points better contact surface is available. The better the contacting, the lower the contacting resistance and the higher the temperature is. Taking this into account, local degradation firstly occurred, which was further distributed. Due to the air starvation, not sufficient amount of oxygen was available for reactions under a specific current density, which was set to be constant. Therefore, oxygen missing for ionic conduction was drawn from the LSCF structure, which is especially visible at points, on which the contacting resistance was the lowest, as can be seen in Fig. 4(a). Next, the temperature increase on such points is possible, which in addition accelerates the morphological degradation of the cathode. Such strong degradation, however, was not stopped at the electrode surface, but was further distributed in order to enable oxygen supply required and resulted in the extensive mechanical damaging of the cathode structure, thus affecting the barrier layer, too, as can be seen in Fig. 4(b). The irreversible degradation and the lost contact between the electrolyte and the cathode resulted in increasing ohmic losses. The cathode preparation and sintering process do not induce such degradation type observed, as visible in Fig. 4(c). It shows the prepared, untreated cathode cross-section, directly after the sintering procedure was finished.

As stated above, when comparing Nyquist plots in Fig. 3(c), the effect of air starvation has obviously increased overall losses shifting the spectrum to the right, and caused both appearing of the third semicircle and strongly rising of the diffusion losses on the cathode side. The THD spectra in Fig. 3(d) show the occurrence of signal distortions with increasing current density. At frequencies higher than 40 Hz, the distortion under air starvation conditions appears to be negligible; as a result, the harmonic analysis is restricted to be shown in the frequency range between 100 Hz and 100 mHz. At a current density of 100 mA/cm^2, under which normal operating conditions are presented, very stable operation can be observed. This case is the same as the one explained in the previous section. Since the measurements are performed on the single-cell level, and not on the separated electrodes, slight distortions are visible as an impact of the processes that occur on both electrodes in parallel, the value of which is lower than 1%. This occurs as a consequence of the non-uniform hydrogen and water vapor (reactant vs. product) distribution along the cells. Therefore, 1% distortion is considered as a threshold value. When this value is exceeded, it refers that undesired changes occur within the system under investigation. Moving towards higher operating current density, thus inducing critical operating conditions, increase of the system non-linearity becomes clear. Non-linear behavior under air starvation conditions can be inferred at frequencies lower than 20 Hz. Rising the operating current density up to 130 mA/cm^2 results in two separated peaks observed between 5 Hz and 10 Hz with a distortion of 3%. At frequencies lower than 2 Hz, an exponential increase is visible in comparison to the reference data observed under 100 mA/cm^2. In this case the maximum distortion of 4% is observed at frequencies lower than 0.3 Hz. Further increase of the operating current intensifies the

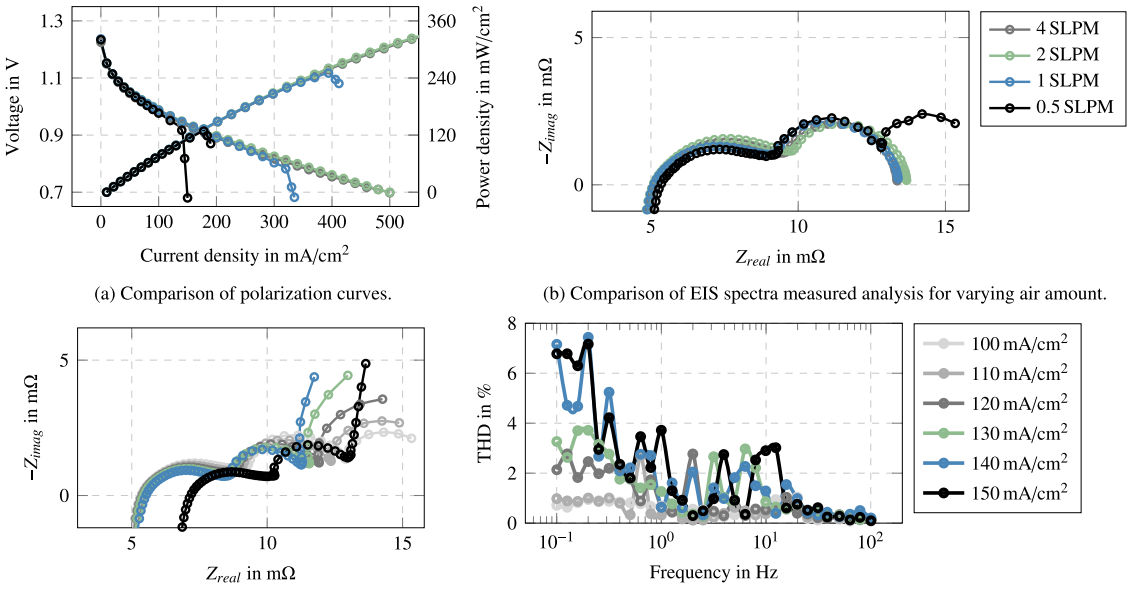

(a) Comparison of polarization curves.

(b) Comparison of EIS spectra measured analysis for varying air amount.

(c) EIS analysis for 0.5 SLPM air and increasing operating current.

(d) THD spectra for 0.5 SLPM air and increasing operating current.

Fig. 3. Comparison of cell performance by reducing air amount and inducing air starvation effect at the operating temperature of 800 °C.

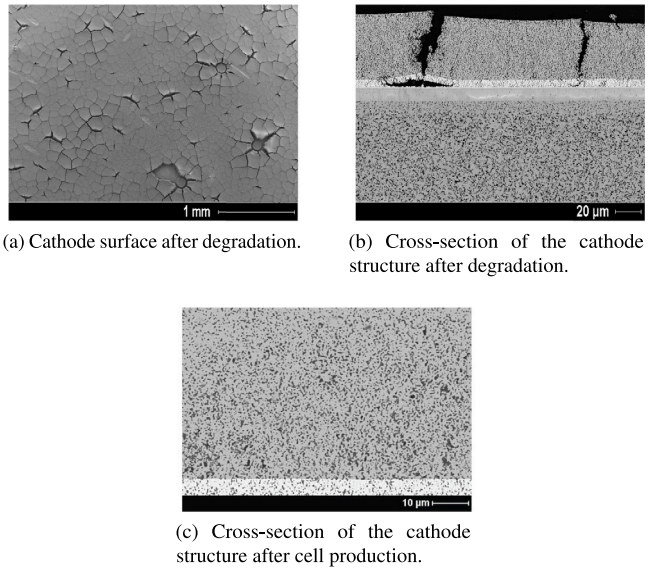

(a) Cathode surface after degradation.

(b) Cross-section of the cathode structure after degradation.

(c) Cross-section of the cathode structure after cell production.

Fig. 4. SEM images of the cathode before and after performed air starvation experiment while supplying the cathode with 0.5 SLPM.

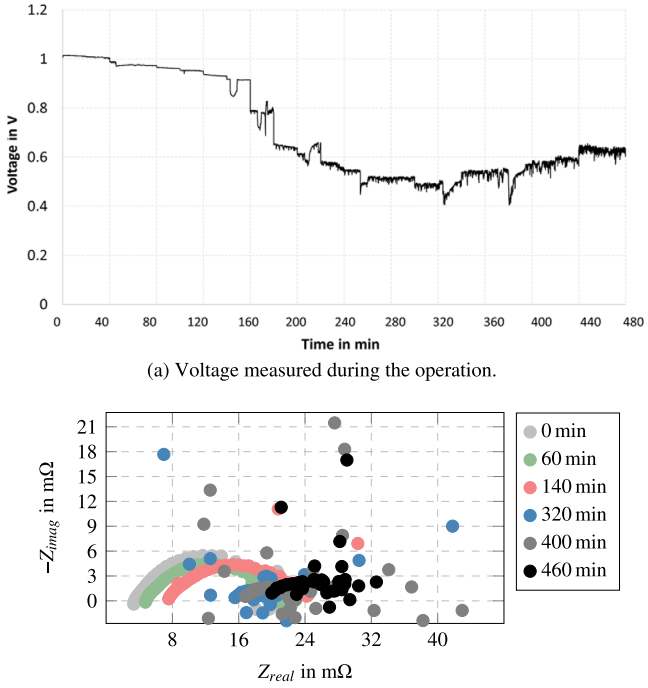

(a) Voltage measured during the operation.

(b) EIS measured during the operation.

Fig. 5. Performance monitoring while fueling SOFC with CH_4/H_2O with S/C = 0.5 for 8 h.

distortions, resulting in the value of even 8%, which refers to the running degradation within the air electrode. Approximately 8% THD was observed at 100 mHz and 5% THD was visible at 18 Hz, respectively, at 150 mA/cm^2. Based on the results achieved, it can be concluded that performing measurements at specific frequencies lower than 20 Hz is sufficient to obtain data related to the cathode degradation, caused by oxygen starvation.

The air depletion effect was as well investigated for BSCF cathodes [10]. In that study, the air supply was firstly sequentially decreased per 0.5 h under constant current density of 180 mA/cm^2, such cycles were repeated 10 times. In contrast to the degradation of the LSCF cathode prepared for the ASC cells used in the present study, the authors showed in [10] that the performed experiments led to slight voltage increase and improvement of the cell performance, which are explained by the increasing porosity of the anode side and reduced amount of steam in the anode pores. However, in general, not much attention has been paid to this degradation phenomenon in the literature, which, as shown in this study, can lead to very fast irreversible SOFC degradation.

3.3. Carbon deposition

Aside from the aforementioned degradation mechanisms, which are based on the insufficient gas supply of either fuel or air electrode,

carbon deposition as a consequence of SOFC operation under carbon-containing fuels was investigated as a further failure mode. For its detailed investigation, carbon formation based SOFC degradation was induced. Since carbon formation is particularly depending on the ratio between the amount of steam and carbon-forming species in the fuel used, water vapor quantity is considered as a relevant accelerating factor, which was varied to intensify the specific degradation mechanisms. To influence degradation time and the amount of carbon formed, SOFC was operated under carbon-inducing atmosphere by: (i) varying S/C ratio when using pure methane as a fuel, and (ii) adding CO as a second carbonaceous fuel component into a gas mixture, thus simultaneously decreasing the S/C ratio. Firstly, methane fuel was used, and S/C ratio was varied between 1 and 0.5. When feeding the SOFC with the fuel with S/C = 1 no degradation was observed at the current density of 50 mA/cm^2, which corresponds to 4 A. In order to accelerate the degradation process, the S/C-ratio was decreased down to 0.5, while the operating current remained unchanged. During the measurement procedure, the cell was operated in a galvanostatic mode for 5 min, after which EIS and THD were measured. The same cycle was repeated 24 times, during which significant deterioration of the cell performance could be identified. Decreasing the S/C-ratio by a factor 2 (from 1 down to 0.5), slight voltage degradation was observed during the first 160 min, as can be seen in Fig. 5(a). At this stage, the degradation trend can be seen as linear and predictable. Nevertheless, after this point, a non-steady behavior of the voltage curve with observable fluctuations became apparent. Voltage monitoring thus enables to give only general information on operating voltage and its behavior as a function of different accelerating factors. In addition, a comprehensive electrochemical analysis was performed during the accelerated SOFC degradation. Electrochemical impedance study, as illustrated in Fig. 5(b), diagnoses increasing resistance as a function of time, whereas the operating conditions remained unchanged. The EIS response showed further increasing instability after 320 min of the SOFC operation under humidified methane. The instability was further emphasized with the increasing operating time. Interestingly, the overall polarization losses decreased, which could be attributed to additional processes that occur in parallel, e.g. direct oxidation caused by mechanical cell damages and increased oxygen partial pressure on the anode side, which thus decreased the overall impedance. During the first 60 min very stable operation was observed, and THD values did not exceed 1%, as indicated by green and gray lines. The first symptoms were determined after 140 min, by measuring the increasing THD-value of 4% at 8 kHz. The deviations in the spectra measured were more prominent with the increasing operating time. The most pronounced peaks were observed at the following frequencies: 2 kHz, 4 kHz and 8 kHz. Induced degradation and the decreasing operating stability increased the THD from 1% up to a maximum of 12% in the frequency range mentioned, as depicted in Fig. 6. Nevertheless, in the low frequency range, thus considering frequencies lower than 15 Hz, a very strong THD increase, of even up to 500%, is observable, as shown in Figs. 6(b) and 6(c). In those two figures the scaling is logarithmic in order to better illustrate the changes observed. As already stated in the previous sections, also here the application of the THD methodology significantly reduces the measurement time from more than 30 min down to several minutes.

In order to improve the visualization and accessibility of the data observed during the long-term operation and to enhance application utility of diagnostic techniques to the customers, we recommend to use the following way of data presentation, as shown in Fig. 7. For such data interpretation, stochastic data analysis is firstly required. This means that numerous samples must be tested under same operating conditions in order to determine the threshold for degradation-free/degradation-inducing operating conditions. In the present study, e.g. pink color is used to outline that the threshold was exceeded and non-desired processes occurred within the cell. When comparing the colors observed, we can estimate if the cell is operated under

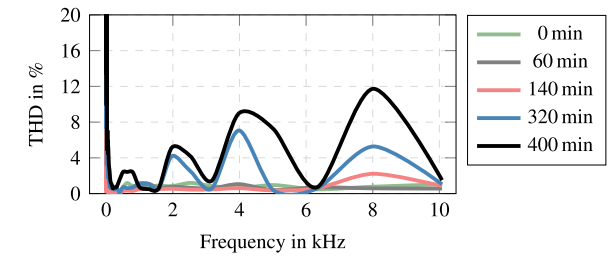

(a) Linear scaling of the THD spectra.

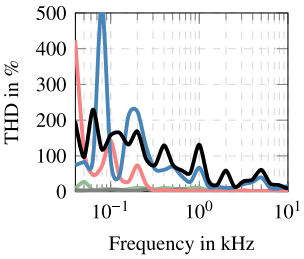

(b) Logarithmic scaling of the THD spectra.

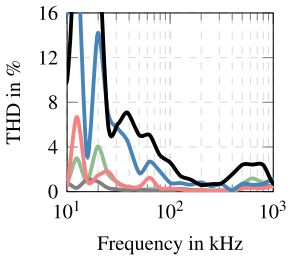

(c) Logarithmic scaling of the THD spectra.

Fig. 6. THD spectra observed during SOFC fueling with methane S/C = 0.5 during 400 min.

safe conditions, and if the safety operation mode is disturbed. Since the SOFC was operated under humidified methane, high non-linearity is expected to be seen at very low frequencies because of several reasons. High steam content in a fuel mixture is the first reason. Furthermore, a number of different reactions can occur when using the above-mentioned fuel mixture; these are steam-reforming, water gas shift reaction, dry-reforming, hydrogen oxidation, but also methane cracking. This means that concentration of gaseous species differs along the cell and it also impacts the temperature distribution making it to be non-uniform. Such behavior is at any case expected for industrial-sized cells and cannot be prevented [37]. Nevertheless, it thus depicts behavior of cells used in stacks and real systems. When comparing the three diagrams in Fig. 7, we can see that in the low and high frequency range (except between 5 kHz and 10 Hz), non-linearity is observable, which is illustrated with THD values >1%. This non-linearity observed does not mean that degradation occurs, but includes all the effects mentioned above as well as time required to reach an equilibrium state.

In diagrams in Fig. 7, on the left-hand side the performance monitored during the 5 h of fueling with methane/steam with a S/C = 1 is shown, while the right-hand side presents the operation under accelerated degradation conditions with S/C reduced to 0.5, during which carbon is expected to be built faster and in a larger amount. Initial performance is very similar, while during fueling with S/C = 1 the performance does not change. However, reduced S/C-ratio shows increasing instability within several hours of operation. If 1% is considered as a threshold it could be assumed that very fast degradation occurs. The instability shown can also occur during reaching the thermodynamic equilibrium of the methane reforming. In order to be able to identify degradation, it is also necessary to set the correct threshold. The conclusion can be made that in this case the threshold has to be increased. Increasing the threshold up to 5%, distortion is observable, as expected, at very low frequencies for both operating conditions, S/C = 1 and S/C = 0.5. When operating the SOFC with S/C = 1, it is clearly shown in Fig. 7 that during five hours, no changes in the system occur. However, by decreasing S/C down to 0.5, we can see intensified distortions after approximately 2 h.

Distortions are visible at frequencies lower than 100 Hz as well as at high frequencies of 2 kHz, 4 kHz and 8 kHz. In order to improve

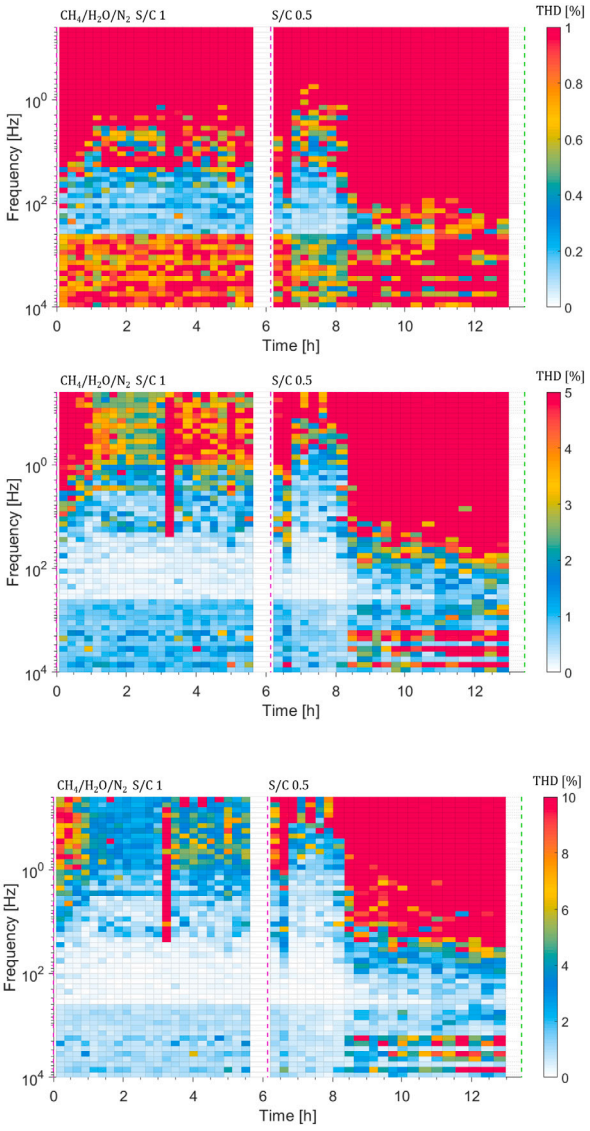

Fig. 7. 2D THD-distribution observed during the SOFC fueling with humidified methane with both S/C = 1 and S/C = 0.5 at the operating current density of 50 mA/cm^2 and the operating temperature of 800 °C.

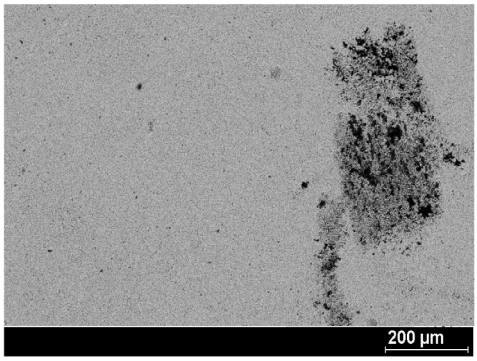

Fig. 8. SEM image of the anode surface after the SOFC fueling with S/C = 0.5.

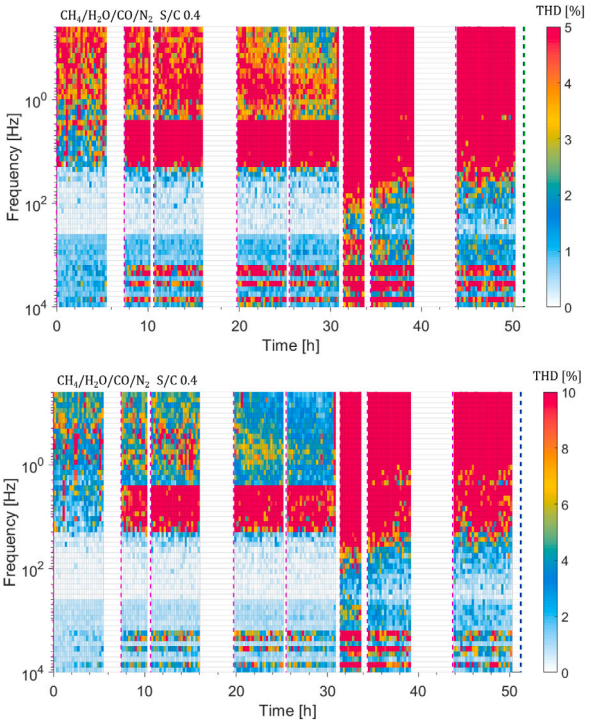

Fig. 9. 2D THD-distribution observed during the SOFC feeding with a $CH_4/CO/H_2O$ mixture with S/C = 0.4 at 800 °C.

the visibility of the undesired failure modes that occurred during the operating time, the threshold value can further be increased up to 10%. In this case, we can see that failure modes started to appear firstly during the SOFC feeding with the methane fuel with S/C = 0.5. However, this would mean the lack of necessary information and therefore 10% distortion is identified to be too high threshold for correct interpretation of the processes within the cell.

Considering all the measurement data shown above we came to the conclusion that degradation mechanisms that occurred caused undesired changes of the cell performance and could lead to irreversible changes. This conclusion is also approved by post-mortem analysis, in which formation of amorphous carbon was identified, as shown in Fig. 8. For initial characterizations, before making final conclusions that can be applied on stacks and real systems, very detailed in-operando analysis and supporting post-mortem analysis are required to be performed.

Accelerated degradation with carbon-containing fuel

Besides the previously shown experiments dedicated to the identification of the carbon deposition phenomenon, one further step was made in this direction. In order to intensify carbon formations and shift the reaction equilibrium by adding the product component to the fuel mixture, CO-component was used to this goal. The S/C-ratio was thus decreased down to 0.4. The online-monitoring of the cell performance was carried out on the way already described above. Here we show the 2D-THD distribution over the operating time, which can be seen in Fig. 9. Two thresholds are selected and presented here, the first one to be 5% and the second one to be 10%. As previously discussed, the threshold should always be identified as a function of operating conditions and gas composition. All the alternations from the steady-state conditions and the threshold defined are thus considered as degradation indications.

The THD-spectra analyzed referred to degradation after less then 10 h, while the voltage monitoring did not show any distinctive variations in the operating voltage. The distortion was observed in the

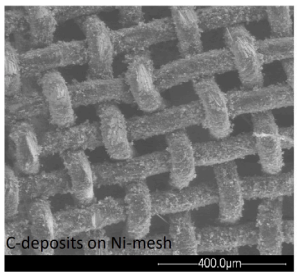

(a) Carbon depositions on the Ni-mesh.

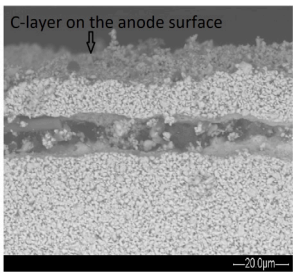

(b) Carbon layer on the anode surface.

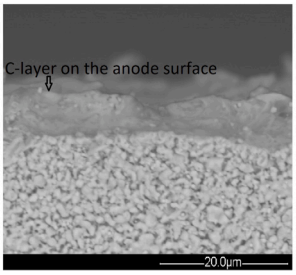

(c) Magnified depiction of the carbon layer on the anode surface.

Fig. 10. SEM images of the anode after the SOFC fueling with S/C = 0.4.

middle-frequency range of between 3 Hz and 10 Hz. However, when operating the cell further without taking any appropriate countermeasures, further failure modes occurred and the degradation intensity increased. After approximately 30 operating hours, significantly increased THDs were observed, but this time the frequency range was extended. This could be linked to the undesired changes within the cell under investigation. In comparison to using humidified methane as a fuel, additional degradation mechanisms were triggered here, which can be associated with the new identified frequency ranges.

After the experiment was finished, post-mortem analysis disclosed intensive carbon depositions, as can be seen in Fig. 10. It is visible that a thick carbon layer covered the complete surface of the contacting Ni-mesh used, whereas on the anode surface a thick layer of solid carbon was formed. The post-mortem analysis was supported by EDX-analysis. It seems that such carbon layer completely disturbs further fuel distribution to the functional layer. Comparing the microstructure of this cell and the previously shown cell after fueling with CH_4/H_2O mixture, microstructure degradation that occurred after fueling with S/C = 0.4 is significantly more pronounced. Considering identification of carbon depositions, the THD analyses showed the most distortions in the same frequency range like in the previous case, which can thus refer to the carbon-related degradation. However, the peak values in the second case, during fueling with the $CH_4/CO/H_2O$ mixture, were significantly higher, thus referring to the higher intensity of the degradation that occurs.

4. Conclusion

This work has clearly demonstrated the potential for application of unconventional online-monitoring tools to identify degradation and damaging operating conditions, that occur during the SOFC operation, already at their preliminary stage. For that purpose, tailored degradation mechanisms were induced and their progression was observed as a function of time. The most relevant failure modes that can occur during the systems operation, such as fuel starvation, air starvation and carbon deposition were taken into account. The work performed here indicated a very promising new diagnosis methodology and data analysis to the fuel cell research field that can be build upon. Moreover, the alternative online-monitoring methods developed here play a significant role in end-of-life predictions and evaluation of accelerated stress testing procedures. Next, we showed that application of conventional characterization tools such as electrochemical impedance spectroscopy can take more than 20 min in specific cases (e.g. when very slow processes occur), while applying the methodology presented in our study, the required time can be reduced down to several minutes, even by a factor of 20. This is of great relevance, since early identification of degradation mechanisms at their preliminary reversible stage enables to take appropriate counteractions and significantly prolong the lifetime of the fuel cell technology.

The measurement techniques and data analysis have only been executed on cell level and the validation of the approach on stack level will be evaluated in a further step. The potential to detect diverse damaging operating conditions and degradation in the SOFC stack will also be evaluated in the future, transferring the knowledge gained up to the higher system levels. Indeed, the validation and verification, and if necessary online recalibration of the method for application in an industrial environment would need to be executed in order to ensure a robust and reliable feedback. The authors also consider additional techniques/approaches to detect the exact time when the specific degradation starts or when it is likely to start.

CRediT authorship contribution statement

Vanja Subotić: Conceptualization, Methodology, Validation, Investigation, Visualization, Data curation, Project administration, Writing original draft, Editing, Funding acquisition. **Norbert H. Menzler:** Resources, Review, Conceptualization. **Vincent Lawlor:** Conceptualization, Review, Funding acquisition. **Qingping Fang:** Review, Conceptualization. **Stefan Pofahl:** Conceptualization, Review. **Philipp Harter:** Visualization. **Hartmuth Schroettner:** Post-mortem analysis. **Christoph Hochenauer:** Funding acquisition, Discussion, Review, Conceptualization.

Declaration of competing interest

The authors declare that they have no known competing financial interests or personal relationships that could have appeared to influence the work reported in this paper.

Acknowledgments

The authors gratefully acknowledge the funding of this project entitled “SOFC-SALT” (Grant No. 853626) by The Austrian Research Promotion Agency (FFG). Furthermore, the authors acknowledge the funding of the project “Degradation monitoring and performance optimization of SOECs” (Grant No. I 3994) by Austrian Science Fund (FWF).

References

[1] Singhal SC, Kendall K. Preface. In: Singhal SC, Kendal K, editors. High temperature and solid oxide fuel cells. Amsterdam: Elsevier Science; 2003, p. xv – xvi.

[2] Barelli L, Bidini G, Cinti G, Gallorini F, Pöniz M. SOFC Stack coupled with dry reforming. Appl Energy 2017;192:498–507. http://dx.doi.org/10.1016/j.apenergy.2016.08.167.

[3] Applicability of the SOFC technology for coupling with biomass-gasifier systems: Short- and long-term experimental study on SOFC performance and degradation behaviour. Appl Energy 2019;256:113904. http://dx.doi.org/10.1016/j.apenergy.2019.113904.

[4] Kim SJ, Choi M-B, Park M, Kim H, Son J-W, Lee J-H, et al. Acceleration tests: Degradation of anode-supported planar solid oxide fuel cells at elevated operating temperatures. J Power Sources 2017;360:284–93. http://dx.doi.org/10.1016/j.jpowsour.2017.06.004.

[5] Fang Q, Blum L, Batfalsky P, Menzler NH, Packbier U, Stolten D. Durability test and degradation behavior of a 2.5 kW SOFC stack with internal reforming of LNG. Int J Hydrogen Energy 2013;38(36):16344–53. http://dx.doi.org/10.1016/j.ijhydene.2013.09.140.

[6] Menzler NH, Sebold D, Guillon O. Post-test characterization of a solid oxide fuel cell stack operated for more than 30,000 hours: The cell. J Power Sources 2018;374:69–76. http://dx.doi.org/10.1016/j.jpowsour.2017.11.025.

[7] Yoon D, Manthiram A. Hydrogen tungsten bronze as a decoking agent for long-life, natural gas-fueled solid oxide fuel cells. Energy Environ Sci 2014;7(9):3069–76. http://dx.doi.org/10.1039/c4ee01455c.

[8] Sasaki K, Li H-W, Hayashi A, Yamabe J, Ogura T, Lyth SM. Hydrogen energy engineering: A Japanese perspective. New Jersey: Springer; 2016.

[9] Gaber C, Demuth M, Prieler R, Schluckner C, Schroettner H, Fitzek H, et al. Experimental investigation of thermochemical regeneration using oxy-fuel exhaust gases. Appl Energy 2019;236:1115–24. http://dx.doi.org/10.1016/j.apenergy.2018.12.046.

[10] Lee T-H, Park K-Y, Kim J-T, Seo Y, Kim KB, Song S-J, et al. Degradation analysis of anode-supported intermediate temperature-solid oxide fuel cells under various failure modes. J Power Sources 2015;276:120–32.

[11] Subotić V, Stoeckl B, Lawlor V, Strasser J, Schroettner H, Hochenauer C. Towards a practical tool for online monitoring of solid oxide fuel cell operation: An experimental study and application of advanced data analysis approaches. Appl Energy 2018;222:748–61. http://dx.doi.org/10.1016/j.apenergy.2018.03.182.

[12] Dolenc B, Boškoski P, Stepančič M, Pohjoranta A, Juričić. State of health estimation and remaining useful life prediction of solid oxide fuel cell stack. Energy Convers Manage 2017;148:993–1002. http://dx.doi.org/10.1016/j.enconman.2017.06.041.

[13] Lang M, Auer C, Eismann A, Szabo P, Wagner N. Investigation of solid oxide fuel cell short stacks for mobile applications by electrochemical impedance spectroscopy. Electrochim Acta 2008;53(25):7509–13. http://dx.doi.org/10.1016/j.electacta.2008.04.047, 7th International Symposium on Electrochemical Impedance Spectroscopy.

[14] Boukamp BA, Rolle A. Use of a distribution function of relaxation times (DFRT) in impedance analysis of SOFC electrodes. Solid State Ion 2018;314:103–11. http://dx.doi.org/10.1016/j.ssi.2017.11.021.

[15] long Wu X, Xu Y-W, Xue T, qi Zhao D, Jiang J, Deng Z, et al. Health state prediction and analysis of SOFC system based on the data-driven entire stage experiment. Appl Energy 2019;248:126–40. http://dx.doi.org/10.1016/j.apenergy.2019.04.053.

[16] Ma R, Liu C, Breaz E, Briois P, Gao F. Numerical stiffness study of multi-physical solid oxide fuel cell model for real-time simulation applications. Appl Energy 2018;226:570–81. http://dx.doi.org/10.1016/j.apenergy.2018.06.030.

[17] Lyu Z, Meng H, Zhu J, Han M, Sun Z, Xue H, et al. Comparison of off-gas utilization modes for solid oxide fuel cell stacks based on a semi-empirical parametric model. Appl Energy 2020;270:115220. http://dx.doi.org/10.1016/j.apenergy.2020.115220.

[18] Sumi H, Yamaguchi T, Hamamoto K, Suzuki T, Fujishiro Y, Matsui T, et al. AC impedance characteristics for anode-supported microtubular solid oxide fuel cells. Electrochim Acta 2012;67:159–65. http://dx.doi.org/10.1016/j.electacta.2012.02.021.

[19] Sumi H, Yamaguchi T, Hamamoto K, Suzuki T, Fujishiro Y. Effect of operating temperature on durability for direct butane utilization of microtubular solid oxide fuel cells. Article Electrochem. 2013;81(2):86–91. http://dx.doi.org/10.5796/electrochemistry.81.86.

[20] Sumi H, Yamaguchi T, Hamamoto K, Suzuki T, Fujishiro Y. High performance of La0.6Sr0.4Co0.2Fe0.8O3–Ce0.9Gd0.1O1.95 nanoparticulate cathode for intermediate temperature microtubular solid oxide fuel cells. J Power Sources 2013;226:354–8. http://dx.doi.org/10.1016/j.jpowsour.2012.11.015.

[21] Ciucci F, Chen C. Analysis of electrochemical impedance spectroscopy data using the distribution of relaxation times: A Bayesian and hierarchical Bayesian approach. Electrochim Acta 2015;167:439–54. http://dx.doi.org/10.1016/j.electacta.2015.03.123.

[22] Liu J, Ciucci F. The Gaussian process distribution of relaxation times: A machine learning tool for the analysis and prediction of electrochemical impedance spectroscopy data. Electrochim Acta 2020;331:135316.

[23] Wan TH, Saccoccio M, Chen C, Ciucci F. Influence of the discretization methods on the distribution of relaxation times deconvolution: Implementing radial basis functions with {DRTtools}. Electrochim Acta 2015;184:483–99. http://dx.doi.org/10.1016/j.electacta.2015.09.097.

[24] Urquidi-Macdonald M, Real S, Macdonald DD. Applications of Kramers—Kronig transforms in the analysis of electrochemical impedance data—III. Stability and linearity. Electrochim Acta 1990;35(10):1559–66. http://dx.doi.org/10.1016/0013-4686(90)80010-L.

[25] Giner-Sanz J, Ortega E, Pérez-Herranz V. Total harmonic distortion based method for linearity assessment in electrochemical systems in the context of EIS. Electrochim Acta 2015;186:598–612. http://dx.doi.org/10.1016/j.electacta.2015.10.152.

[26] Kadyk T, Hanke-Rauschenbach R, Sundmacher K. Nonlinear frequency response analysis of PEM fuel cells for diagnosis of dehydration, flooding and CO-poisoning. J Electroanal Soc 2009;630(1):19–27. http://dx.doi.org/10.1016/j.jelechem.2009.02.001.

[27] Mao Q, Krewer U. Total harmonic distortion analysis of oxygen reduction reaction in proton exchange membrane fuel cells. Electrochim Acta 2013;103:188–98. http://dx.doi.org/10.1016/j.electacta.2013.03.194.

[28] Mao Q, Krewer U. Sensing methanol concentration in direct methanol fuel cell with total harmonic distortion: Theory and application. Electrochim Acta 2012;68:60–8. http://dx.doi.org/10.1016/j.electacta.2012.02.018.

[29] Steffy N, Selvaganesh SV, L. MK, Sahu A. Online monitoring of fuel starvation and water management in an operating polymer electrolyte membrane fuel cell by a novel diagnostic tool based on total harmonic distortion analysis. J Power Sources 2018;404:81–8. http://dx.doi.org/10.1016/j.jpowsour.2018.10.012.

[30] Thomas S, Lee SC, Sahu A, Park S. Online health monitoring of a fuel cell using total harmonic distortion analysis. Int J Hydrogen Energy 2014;39(9):4558–65. http://dx.doi.org/10.1016/j.ijhydene.2013.12.180.

[31] Malafronte L, Morel B, Pohjoranta A. Online total harmonic distortion analysis for solid oxide fuel cell stack monitoring in system applications. Fuel Cells 2018;18:476–89. http://dx.doi.org/10.1002/fuce.201700230.

[32] Menzler NH, Malzbender J, Schoderböck P, Kauert R, Buchkremer HP. Sequential tape casting of anode-supported solid oxide fuel cells. Fuel Cells 2014;14(1):96–106. http://dx.doi.org/10.1002/fuce.200800153.

[33] Schafbauer W, Menzler NH, Buchkremer HP. Tape casting of anode supports for solid oxide fuel cells at Forschungszentrum Jülich. Int J Appl Ceramic Technol 2014;11(1):125–35. http://dx.doi.org/10.1111/j.1744-7402.2012.02839.x.

[34] Szász J, Wankmüller F, Wankmüller W, Wilde V, Störmer H, Gerthsen D, et al. Nature and functionality of La 0.58 Sr 0.4 Co 0.2 Fe 0.8 O 3-δ / Gd 0.2 Ce 0.8 O 2-δ / Y 0.16 Zr 0.84 O 2-δ Interfaces in SOFCs. J Electrochem Soc 2018;165(10):898–906. http://dx.doi.org/10.1149/2.0031811jes.

[35] Fang Q, Blum L, Peters R, Peksen M, Batfalsky P, Stolten D. SOFC Stack performance under high fuel utilization. Int J Hydrogen Energy 2015;40(2):1128–36. http://dx.doi.org/10.1016/j.ijhydene.2014.11.094.

[36] Schluckner C, Subotić V, Lawlor V, Hochenauer C. Three-dimensional numerical and experimental investigation of an industrial-sized SOFC fueled by diesel reformat – part i: Creation of a base model for further carbon deposition modeling. Int J Hydrogen Energy 2014;39(33):19102–18.

[37] Subotić V, Schluckner C, Mathe J, Rechberger J, Schroettner H, Hochenauer C. Anode regeneration following carbon depositions in an industrial-sized anode supported solid oxide fuel cell operating on synthetic diesel reformate. J Power Sources 2015;295:55–66. http://dx.doi.org/10.1016/j.jpowsour.2015.06.133.